

PROPOSED MODELING APPROACH OF WELDING PROCEDURES FOR HEAVY STEEL PLATES

Omar A. Ibrahim ¹, Dimitrios G. Lignos ² and Colin A. Rogers ³

¹Ph.D. Candidate. Dept. of Civil Engineering and Applied Mechanics McGill University
Macdonald Engineering Building 817 Sherbrooke Street West Montreal, QC, Canada, H3A 0C3
email: omar.ibrahim@mail.mcgill.ca

²Corresponding author
Associate Professor. Dept. of Civil and Environmental Engineering, Ecole Polytechnique Fédérale
de Lausanne (EPFL)
EPFL ENAC IIC RESSLab, GC B3 485, Station 18, CH-1015 Lausanne, Switzerland
email: dimitrios.lignos@epfl.ch
Tel. +41 21 693 2427
Fax. +41 21 693 2868

³Associate Professor. Dept. of Civil Engineering and Applied Mechanics McGill University
Macdonald Engineering Building 817 Sherbrooke Street West Montreal, QC, Canada, H3A 0C3
email: colin.rogers@mcgill.ca

Abstract

A numerical modeling approach is proposed to assess the effectiveness of automatic submerged arc welding procedures for steel plates with thickness larger than 50mm. The scope of study includes partial joint penetration butt welds, their numerical analysis, and the subsequent development of welding recommendations for thick steel plates, with the ultimate objective to reduce the related industrial losses. The proposed approach consists of a heat-transfer numerical model that is integrated with a stress analysis model that was validated with measurements obtained from two heavy steel assemblies that were welded in a fabrication shop. The first consisted of two 75mm thick plates welded in the flat position, for which temperature measurements were recorded. The proposed model shows good agreement with these measured temperature results. The second consisted of a built-up box column that also utilized 75mm thick plates. This assembly experienced cracks near the welds after the completion of the welding procedures. Through a comprehensive investigation of the material properties of the steel plates it was confirmed that the material met the specifications in terms of minimum fracture strain elongation and fracture toughness. The model was used to successfully predict the crack initiation due to thermal stresses that were developed near the welds. The proposed model can potentially be employed to assess the defect limits found in current specifications for welded steel assemblies that utilize thick plates.

Keywords: Steel, thick plates, butt welds, welding simulation, creep modeling, heat transfer analysis

1 Introduction

Welding is a commonly used method for joining structural steel components. This is attributed to the reliability of the connection, its structural simplicity in terms of load transfer and its cost effectiveness. However, welding can also be problematic; a primary example is that the process is accompanied by residual stresses. These stresses develop in the plates being welded because of the uneven heat expansion and the subsequent contraction upon cooling, both of which are often constrained by the configuration of a structural member's or connection's cross-section. In recent years, the use of thicker built-up members and heavier steel shapes have been preferred for the construction of complicated structural systems having long spans, greater heights and larger loads due to more demanding design and performance requirements [1]. The use of thick plates further exacerbates the development of weld related residual stresses because of the greater constraint to the steel's expansion and contraction; as a result, there is an increased likelihood of crack development originating from discontinuities and imperfections. Design codes and specifications [2-5] provide guidance for the welding processes to ensure the integrity of the welded assembly. However, the available guidelines were developed based on commonly used less than 25mm thick structural steel plates. The relevant North American design specifications [2-5] account for the aspects introduced by Miller [6] to reduce the intensity of residual stresses induced by the welding procedure; however, these are mostly qualitative recommendations to reduce the restraint placed on the connection and to ensure that minimum material fracture toughness levels are met. Cases of structural failure have been reported due to failure in welded thick steel plates assemblies [7]. Recently, based on feedback from one of the largest steel fabricators in North America; it was

required to scrap over 400 tons of thick steel plates that developed unrepairable cracks after welding, with total industry losses exceeding \$1M. Given this current situation, the specifications for the welding procedures and the acceptance criteria for cracks and discontinuities for thick steel plates (greater than 25mm) [2-5] are required to be updated. In order to do so, one of the first requirements is to develop a practical numerical approach from which one can examine the effect of different welding procedures on thick steel plates and the resulting residual stresses. It is necessary for this tool to comprise the features of the welding procedure, i.e. the welding temperature, the welding travel speed and the preheat/inter-pass temperatures, as well as the steel's time and temperature dependent material properties.

A summary of related laboratory and analytically based studies is provided herein. Bjorhovde et al. [8] conducted an extensive testing program using the sectioning method to measure the residual stresses induced in 50mm ASTM A36 Gr. 36 [9] plates ($f_y = 250$ MPa) from rolling, flame cutting and welding. The results of these tests showed that the residual stress post fabrication near the welded area can be as high as the yield stress of the steel. Fisher et al. [10] detected cracks in a W360x1086 ASTM A572 Gr. 50 [11] section ($f_y = 345$ MPa) spliced with groove welds; the high residual stresses induced by the web groove welds initiated crack instability. The authors recommended using fillet welds instead of butt groove welds to avoid welding near the k-area of jumbo W-sections, which had revealed weak fracture toughness of $35 \text{ MPa}\cdot\sqrt{\text{m}}$ at 0°C compared to the AWS D1.1 Specification [2] limit of $58 \text{ MPa}\cdot\sqrt{\text{m}}$ at 0°C . In other research programs the investigation of the effects of the employed welding procedure on steel plates has also been conducted numerically. For example, Brickstad et al. [12] developed a numerical simulation for

the welding procedure of 40mm thick stainless steel nuclear piping systems, of 230 MPa yield stress, to investigate the through-thickness variation of axial and hoop stresses and to assess the growth of surface flaws at circumferential butt joints. Acevedo et al. [13] conducted experimental and numerical assessment of residual stresses induced by welding at the region surrounding the toe of a tubular K-shaped joint. The residual stress measurements were conducted through Neutron-diffraction of welded tubes of thicknesses 20mm and 8mm. The numerical simulation comprised an uncoupled thermo-mechanical model, which was validated with the experimental data; analytical residual stress distribution equations were also developed. Nikolaidou et al. [14] used an uncoupled thermo-mechanical model to investigate the cause of crack initiation after welding a 25mm doubler plate to the web of a W360x237 column of high strength A913 Gr. 65 450MPa steel [15]; the investigation proved that high residual stress induced by the welding procedure resulted in the detected cracks. Further, an uncoupled thermo-mechanical was developed by Lee et al. [16] to produce an assessment of the residual stresses of butt welded 25mm thick plates and to study the relaxation phenomena accompanied by post-welding cyclic loading. The residual stress outputs from their model were validated by means of the results from a test program [17]. The uncoupled thermo-mechanical model effectively predicted the residual stresses for the 25mm thick plates.

It is not practical to rely solely on an experimental study of the welding procedure of thick plates in order to improve current welding procedures of heavy assemblies due to the required large-scale weld tests and significant number of parameters to be investigated. Therefore the development and use of a numerical simulation of typical welding procedures for thick plates was justified. This

paper describes a numerical uncoupled thermo-mechanical modeling approach which can be used to investigate the effect of the welding procedures on steel assemblies that utilize thick plates (> 50mm) and heavy cross-sections. The simulation was validated with a coordinated experimental program that consisted of three phases; the first phase included the validation of the temperature distribution results from the numerical model with the temperature measurements from the welding procedure of two 75mm thick ASTM A572 Gr.50 [11] steel plates. The second phase was the validation of the resultant residual stress distribution with experimental results obtained by Chen and Chang [18]. The third phase included the application of the modeling approach to assess the influence of the employed welding procedure for a heavy built-up steel box column, fabricated from the same heat of steel plates studied in the first phase. Cracks were observed in this column after the welding procedure had been completed.

2 Proposed modeling approach for welding procedures

The aim of numerically simulating a welding procedure is to make it possible to use a practical approach to investigate the likelihood of crack propagation, as well as the influence of different welding procedures. A numerical simulation for the welding procedure has to comprise the effects of elevated temperatures on the steel plates and must provide the generated stress from the temperature change. The elevated temperatures change the crystalline structure of the steel material and, correspondingly, its properties (e.g., strength and stiffness). Because our interest is the magnitude of the generated residual stresses from the welding procedure, it is feasible to only include the changes of the mechanical properties of the steel material at elevated temperatures and to disregard the changes in the crystalline structure, since it is inherently incorporated in the

strength change; this assumption has been also considered in previous research [12-14, 16]. The proposed finite element (FE) approach is demonstrated through detailed modelling of the welding of a 75mm thick built-up box column and two 75mm thick steel plates, using ABAQUS 6.11 [19] for 3-dimensional (3-D) modeling. The FE simulation is divided into two phases. The first phase is a simulation of the heat transfer from the welding procedure through the base metal to obtain the temperature distribution over time. The second phase involves a stress analysis model (or a visco-plastic model to account for potential creep strain effects) to determine the stresses induced by the welding procedure. The two phases were then integrated to simulate the welding procedure.

The element “death and birth” technique, as described by Brickstad and Josefson [12], was incorporated in the FE model. This technique is used to deactivate and reactivate the elements representing the welding beads to simulate the addition of new material to the connection during fabrication. As an example, Figures 1a-1b show the activation of only the first six passes at each corner of the built-up box column 3-D model shown in Figure 2a, while the remaining weld passes are deactivated. To achieve this, the “Model Change” interaction in ABAQUS 6.11 [14] was utilized such that prior to the deactivation step the forces/heat-fluxes that the region to be removed exerts on the surrounding nodes are ramped down to zero. Therefore, the effect of the removed region on the rest of the model is completely absent only at the end of the deactivation step. To reactivate a welding pass the same interaction is used with the “strain free” option in ABAQUS 6.11 [19] such that at the start of the weld pass it provides a zero strain contribution to the simulation. The two simulation phases are discussed in detail in Sections 2.1 and 2.2. The mesh sensitivity study and element selection of the FE models in the proposed approach are described

in Section 2.3. Additionally, the effect of introducing creep strain properties on the residual stress results is discussed in detail in Section 2.4.

2.1 Heat transfer simulation

The heat transfer simulations for the built-up box column and the two steel plates were generated as illustrated in Figures 1a and 1c, respectively. The finite element mesh at the welding area as well as the welding passes for both cases are shown in Figures 1e-1f respectively. To achieve the resulting temperature distributions, the following steel material properties were considered: the thermal conductivity and the specific heat, as well as the effect of elevated temperatures on their values. The values of these properties were defined according to the “Society of Fire Protection Engineers” SFPE Handbook for Fire Protection [20] as shown in Table 1. All the welding passes were explicitly created in the finite element model; however, they were deactivated at the first step of the analysis. Each pass was simulated in three steps; 1) heating of the welding area, for the considered pass, up to the welding temperature (1500°C), 2) activating the weld pass elements, and 3) cooling of the steel through natural convection until the preparation for welding of the next pass was finished. This was achieved by defining conduction and radiation contact surfaces between the steel and surrounding air of 20°C ambient temperature; considering a heat transfer coefficient of 25 W/m²K [20] and an emissivity coefficient of 0.625 according to Eurocode 3 Part1.2:2001 [21], which is in the range specified by ANSI/AISC 360-10 [3] for structural steel components (0.5 - 0.7). However, the heat transferred by radiation is negligible to that transferred by conduction and convection. The traveling heat source is simulated by dividing the traveling

distance into a finite number of divisions, such that the heat is applied through a boundary condition of ramp heating from the preheat temperature to the welding temperature to each division according to the travel speed. The heating of each division starts at the end of heating of the previous division.

2.2 *Stress analysis model*

The stress analysis FE model imports the temperature distributions obtained from the heat transfer simulation at every increment during the heating and cooling of each weld pass. Using the thermal expansion coefficient, at the corresponding temperature, the change in temperature is transformed to strains, which are then transformed to the corresponding stresses as shown in Figures 1b and 1d. A multi-linear plasticity model and geometric nonlinearities are considered in the stress analysis model. The Von Mises yield surface is utilized in ABAQUS to simulate the isotropic metal plasticity. The material properties, at elevated temperatures, required for this analysis are the elastic modulus, the yield stress, the yield strain, the ultimate stress, the ultimate strain and the coefficient of thermal expansion. The welding procedure applies temperatures to the base metal as high as the melting point of steel (1500°C). At such temperature the steel is at a liquid phase that has negligible stiffness and strength. As the steel temperature decreases the material transforms through different phases to reach its solid phase at room temperature; during these phase transformations the mechanical and thermal material properties of steel change gradually. Figure 3 illustrates the values for the material properties used in the stress analysis model.

The reduction factors for the material properties, due to elevated temperature, were set according to AISC 360-10 [3] and the SFPE Handbook of Fire Protection [20]. The chosen reduction factors were similar to those measured by Hu et al. [22] for ASTM A992 steel [23]. The weld metal properties were assumed as F7A4-EM12K according to AWS D1.1 A5.17 [2], which is typically used for a SAW procedure. The base metal properties were obtained from tensile tests of the plate material, which are discussed in Section 3.1.1.

2.3 Mesh sensitivity study and selected finite element types

The solution of the proposed FE model is conducted using the ABAQUS implicit solver. The Euler backward method is utilized by ABAQUS for solving transient problems, which is unconditionally stable for linear finite elements [19]. As such, linear elements were selected for the proposed FE model, specifically C3D8 elements for the 3-D model, which are 8-node linear isoparametric elements with full integration. A mesh sensitivity study was conducted for the proposed FE model to evaluate the optimum mesh size, in terms of accuracy and calculation speed, to be employed for the heat and stress analyses. As the ability of the finite element to transfer the applied heat and undergo deformation is required to be studied, this can be established regardless of the model size and plate thickness. A quarter section of a box configuration composed of 28 mm thick plates connected with a complete joint penetration (CJP) weld comprising 10 weld passes was utilized for the mesh sensitivity study. The mesh size varied from a maximum element dimension of 20mm to 5mm. Shear locking was avoided because the deformations in this analysis are very small compared to the size of the model; also, quadratic elements were tested and showed no significant difference in the results from using linear elements. Hour-glassing was avoided by using full

integration and by comparing the results with those of models built with quadratic elements. From this study, the selected mesh for the 3-D model was of minimum element size 2mm and maximum 9mm, such that the difference between the maximum stresses of this mesh size and the denser mesh was less than 15%. Figure 4 shows the Von Mises stress distribution sensitivity to the mesh size and the mesh selected for this study.

2.4 *Creep strain modeling*

The effect of creep strain on the resulting residual stresses was investigated such that the welding simulation better accounts for the behaviour of the steel material. Creep is the increase in strain with time under a constant tensile load, as illustrated in Figure 5a. Creep effects on steel are only significant at elevated temperatures. The creep strain is divided into three stages; the primary, the secondary and tertiary creep [24]. The primary creep is for a short duration and is characterized by a decreasing strain rate. The secondary creep has the longest duration and has a constant strain rate (it is the minimum strain rate at a constant temperature and stress). In the tertiary stage the strain rate increases rapidly until fracture. Creep is commonly studied in steel structures such as nuclear power plants and oil refineries where stainless steel is used and high temperatures are experienced [20]. Consequently, the available creep test results for steel are mostly for austenitic stainless steel. The temperature at which the creep becomes significant in steel is called the homologous temperature [25]; it is when the ambient temperature is greater than 0.3 to 0.5 of the absolute melting temperature of the material [25]. As such, the creep strain becomes significant for steel at ambient temperature greater than 400°C.

Creep strain is always accompanied by two other phenomena; the creep strain recovery and the stress relaxation [25]. The creep strain recovery takes place when the load is removed; first the elastic strain is recovered, then part of the creep strain is recovered leaving the permanent strain as shown in Figure 5b. Stress relaxation is the decrease of the stress with time under constant strain as shown in Figure 5c. The loading type also has an effect on the creep strain according to Faruque et al. [26]. The temperature in the base metal exceeded the homologous temperature of the material only for a short period during the welding procedure simulations. As a result, the present paper is only concerned with the primary and secondary creep stage. Creep tests were conducted by Lee et al. [27] to evaluate the creep curves of ASTM A992 steel [23] between the temperatures 400 and 1000 °C. The data from these tests were used to develop empirical equations describing the creep strain of the steel at different temperatures. The multi-axial creep was considered using two approaches. First according to Boresi et al. [28], where the equivalent stress was considered as a combination of the Von Mises stress and the deviatoric stress (noted as “creep-1”). In the second approach the equivalent stress is a combination of the Von Mises stress and the maximum principal stress according to Goyal et al. [29] (noted as “creep-2”). Equations 1 and 2 show the approaches developed in this research using constants developed by nonlinear regression of the test data obtained from Lee et al. [30].

$$\varepsilon_{cr} = 2.125e-04 \times e^{\frac{-11111}{T}} \sigma_{vm}^2 S_{dev} \times \Delta t \quad \text{For creep-1} \quad (1)$$

$$\varepsilon_{cr} = \frac{3}{2} (2.125) \times e^{-04} \times e^{\frac{-11111}{T}} (0.9\sigma_{vm} + 0.1\sigma_1)^3 \times \Delta t \quad \text{For creep-2} \quad (2)$$

Where, ε is the creep strain; T is the temperature [$^{\circ}\text{C}$]; σ_{vm} is the von Mises stress [MPa]; S_{dev} is the deviatoric stress [MPa]; σ_1 is the maximum principal stress [MPa]; and Δt is the time increment of the solution procedure [sec]. A FORTRAN subroutine was developed in ABAQUS [19] in order to incorporate the time dependent strain properties of steel in the proposed FE model. In this subroutine the two approaches stated above were implemented. Figure 6 shows a comparison of the resulting stresses from the welding procedure with and without creep strain considerations. The differences in the resulting maximum stresses are 4% and 8% for modeling approaches creep-1 and creep-2, respectively. The resulting maximum stresses considering the creep strain were always lower than those obtained without considering it. The reason for this is that the base metal did not experience temperatures above the homologous temperature of steel (400°C) for an adequate duration to develop creep strains. Moreover, in most of the results, stress relaxation took place, which was more significant than the stress change due to the creep strains. However, if a welding procedure utilizes a heat input that is much higher than the commonly used value (2 to 3 KJ/mm) the creep strain may become more influential.

In conclusion, considering the creep strains in the welding procedure simulation showed a very small change in the maximum stress results, neglecting the creep strains proved to be more conservative than incorporating them. Furthermore, the computational time required to analyze a FE model considering creep is more than double that required for a model without creep. For these reasons the creep strain properties were neglected from the final welding procedure simulations presented in this paper. However, for welding procedures involving heat input higher than

commonly used in practice, it is recommended to take into account the effect of creep strains on the resultant stresses.

3 Experimental validation of the proposed modeling approach for welding procedures

The proposed numerical modeling approach for welding procedures of heavy steel assemblies that utilize thick plates requires validation with relevant experimental data for both the heat transfer and stress analysis simulation phases. Three case studies were adopted for this validation. The first case study involved temperature measurements during the welding of two 75mm thick ASTM A572 steel grade 50 ($f_y = 345$ MPa, $f_u = 450$ MPa) [11] plates (Figure 7a); these measurements were used to validate the heat transfer simulation. For the validation of the stress distribution results of the proposed modelling approach, the second case study involved the simulation of the welding simulation of a box section, of A572 steel grade 50 ($f_y = 345$ MPa, $f_u = 450$ MPa) [11], that underwent an experimental procedure to evaluate the residual stress distribution developed from the welding procedure by Chen and Chang [18]. The third case study was of a heavy built-up box column (Figure 2a) fabricated from 75mm thick steel plates of the same material (heat) as the first case study. This third case study is used to demonstrate how the proposed modeling approach can be incorporated in an assessment of the welding procedure (Section 3.4). The plates that were used for testing were originally intended for use in box columns that were eventually scrapped due to the development of cracks discovered during fabrication and, in particular, after welding. The scrapped plates were used for material tests to calibrate the FE model (Section 3.1).

3.1 Material tests for characterizing the properties of the built-up box columns

Tensile and Charpy-V-Notch (CVN) specimens were extracted from the box-column specimens retained by the fabricator to evaluate the material properties, and to determine the effect on these properties of the welding procedure at different stages. The measured material properties were also used to calibrate the corresponding FE model. This included a fully welded built-up box column (13 weld passes at each corner), a partially welded column (6 weld passes at each corner) and a non-welded plate as shown in Figure 8. A total of 74 tensile coupon and 100 CVN specimens were extracted from all the box-column and plate specimens at different locations within the thickness of the steel plates. The results were categorized into four groups regarding the location of the CVN and tensile coupon specimens; 1) near the weld and on the plate surface, 2) near the weld and through the plate thickness, 3) away from the weld and on the plate surface and 4) away from the weld and through the plate thickness. Figure 9 shows a sample of the different locations of the tensile and CVN specimens extracted from the fully welded column, the partially welded column and the non-welded plate.

3.1.1 Tensile coupon test results

The effect of the thickness of the welded plates and the welding procedure on the engineering stress-strain response of the steel material was assessed based on the tensile coupons that were extracted from the built-up box columns at the locations shown in Figures 9a-9c. The engineering stress-strain curves from the 74 tensile tests, carried out according to ASTM A370 [31], are

presented in Figure 10. A summary of the resulting mechanical properties of the steel material, according to the four classifications mentioned in Section 3.1, is shown in Table 2.

Based on Figure 10 and Table 2, the yield stress (f_y) and the ultimate stress (f_u) values were found to be greater than the nominal values according to the specifications for A572 Gr. 50 steel [11]. However, the welding procedure and plate thickness affected the engineering strain at fracture. In particular, for tensile coupons located through the thickness of the steel plate the average engineering strain at fracture was 0.16, and for the specimens near the weld it was 0.15. These values are lower than what is expected from ASTM A572 Gr. 50 steel; for which the minimum elongation is 0.18 [11].

Specimens away from the weld and at the surface of the plate complied with the minimum elongation requirements per [11]; the reason for this is that the area of steel from which these specimens were obtained was less affected by the welding and the lack of compactness of the steel grains from the rolling process that occurs at the through thickness regions of thick plates. Note that coupons extracted from the plate surface and away from the weld showed a low coefficient of variation (COV) for plastic strains compared to the ones that were extracted from the location through the plate thickness and near the weld.

3.1.2 Charpy-V-Notch test results

The CVN tests, conducted according to ASTM A370 [31], provided values of the energy required to break a notched specimen. The fracture toughness of the steel material was computed from the CVN energy value depending on the testing temperature and the material's elastic modulus [32].

The 100 CVN specimens that were extracted from the box-columns were tested at temperatures of -60, -40, 0, 60 and 81 °C in order to develop the fracture toughness profile of the steel material. Specimens were taken from different locations through the thickness of the 75mm steel plates of the built-up box columns (Figures 9d-9f). The average CVN absorbed energy per location through the thickness of the respective steel plates is shown in Figure 11. A summary of the resulting absorbed energy values of the steel material, according to the four classifications, mentioned in Section 3.1, is summarized in Table 3. Figure 11 also shows the theoretical CVN-temperature curve based on the equivalent carbon content of the material according to Johnson et al. [27].

It is seen from Figure 11 that the average test results are very close to the theoretical CVN-temperature curve. The material's fracture toughness relation with temperature is divided into three portions; lower shelf values at low temperatures that are characterized by low fracture toughness values and small variations; upper shelf values at high temperatures that are characterized by high fracture toughness and small variations; and the transition zone values between the previous two portions, which are characterized by rapid linear variation in the fracture toughness values with temperature. The results are in agreement with the code requirements [2-5], which state that a CVN value for ASTM A572 Gr. 50 steel should not be lower than 27 joules at 0°C.

However, the CVN results show a very high COV at lower shelf temperatures (Table 3), which reveals high variability in the obtained CVN values from the same location category and correspondingly, the fracture toughness of the material. Additionally, specimens near the weld and through the thickness showed low CVN values compared to specimens near the weld and at the plate surface at the same temperatures. This can be attributed to the fact that the through thickness

grain sizes are greater than those at the surface [33], hence, the effect of the heat affected zone on the material toughness is greater at the through thickness region [34].

3.2 Case Study-1: Temperature measurements

In order to validate the results from the heat-transfer analysis of the proposed modeling approach discussed in Section 2 a testing program was established using two steel plates of the same material (heat) as the heavy built-up box column to perform temperature measurements during the welding procedure. The test layout is shown in Figures 7b-7c. The welding was conducted using an automatic submerged arc welding (SAW) procedure with average heat input of 3 KJ/mm, average current of 850 A and average voltage of 30 V. Each side was welded with a partial joint penetration (PJP) weld, with groove depth of 19mm and groove angle of 60°, consisting of 6 passes (Figure 7b). The electrodes and flux used for this procedure were F7A4-EM12K according to AWS D1.1 A5.17 [2]. Two electrodes were used with diameter 2.4mm and an 8mm gap. The average travel speed of the electrodes was 500 mm/min and the average wire feeding speed was 320 cm/min. The region to be welded and its surrounding area, at a distance equal to 75mm from both sides of the weld, measured from the edge of the weld, was pre-heated to 110 °C as specified by AWS D1.1 “Table 3.2” [2]. Once the welding passes had been completed on the first side (noted as “Side 1” in Figure 7b), the two plates were flipped and then the welding of the other side was completed (noted as “Side 2” in Figure 7b). During each welding pass temperature measurements were obtained at three locations (T1, T2 and T3) as illustrated in Figure 7c using an infrared radiation thermometer, with accuracy $\pm 1\%$ of reading and adjustable emissivity, at a 20 seconds time interval, the temperatures were also measured using a digital welding pyrometer with surface probe

for validation of the results and it showed agreement with the results of the infrared thermometer. The closest measurements to the welding line were at 20mm due to the large amount of flux during the welding process. Figure 7d shows the final weld beads after completion of the welding procedure. Figure 12 shows the measured temperatures at T1 and T2 during the welding of passes 3 and 5. The measured temperatures at location T1 were constant as the welding electrode approached this position. The temperature readings started to increase as the welding electrode passed T1. At location T2 the measured temperatures were largely constant through the welding procedure of each pass since it was away from the heat source by 40 mm. The temperature did, however, start to increase near the completion of the pass once the heat flow from welding was able to traverse this additional distance.

3.2.1 Validation of the heat-transfer simulation

In order to establish confidence in the results of the FE simulation for the welding procedure; temperature distributions were obtained from the 3-D FE model of case study-1 at the same locations that were extracted from the test. Figure 12 shows a comparison of the temperature results between the FE model and the measured temperatures at locations T1, T2 and T3 (Figure 7c) during the weld passes 3 and 5 (Figure 7b). The welding simulation traced the temperature results of the weld experiments with a maximum absolute relative error of 20% at T1 and negligible for T2 and T3. This is in part attributed to the amount of the welding flux deposited on the steel plates from the SAW procedure, which made it a challenge to obtain precise temperature measurements at location T1 that was very close to the weld (Figure 7c).

3.3 *Case study 2: Stress distribution validation*

An experimental evaluation of the welding residual stresses was conducted for an ASTM A572 Gr.50 [11] steel box-section of dimensions 500x500x1000x28 shown in Figure 13a by Chen and Chang [18]. The sectioning method was used at the mid-length of the welded component to compute the residual strains using strain gauges of 250mm gauge length. A FE simulation of the welding procedure was developed utilizing a typical welding procedure for this complete joint penetration (CJP) assembly; such that the number of passes was 10, welding travel speed was 2.5mm/s and no preheat was performed. The material model in the simulation was updated according to the tensile test results conducted by Chen and Chang [18] for the same box-section material. Figure 13b shows the resultant residual stress distribution on the surface of the welded 28mm plate from the FE simulation. The stress distribution at the path at mid-length of the welded plate in the FE simulation, as shown in Figure 13b, is compared to the residual stress results from the sectioning test conducted by Chen and Chang [18]. A comparison of the residual stress distribution at the mid-length of the welded plate between the FE results and the experimental results is shown in Figure 13c. The proposed method for welding procedure simulation of thick steel plates traced the experimental peak tensile residual stress values with a maximum error of +8%.

3.4 *Case study-3: heavy built-up box column*

A simulation of the welding procedure for the second case study heavy built-up box column (Section 3) was also carried out. The fabricator followed the recommendations given by AWS

D1.1 2010 “Clause 3 for prequalification of Welding Procedure Specifications (WPS)” [2] for welding thick plates, however, extensive cracking still occurred after the completion of the welding procedure. The welding procedure was conducted on two corners of the built-up column simultaneously using an automatic SAW procedure with average heat input of 2.4 KJ/mm, average current of 700 A and average voltage of 30 V. Each corner was a PJP weld, with groove depth of 37.5mm and groove angle of 60°, consisting of 13 passes (Figure 2b). The electrodes and flux used for this procedure were F7A4-EM12K according to AWS D1.1 A5.17 [2]. Two electrodes were used at each corner with diameter 2.4mm and an 8mm gap. The average travel speed of the electrodes was 525 mm/min and the average wire feeding speed was 255 cm/min. For this case-study, the welding sequence according to the fabricator and the AISC welding guidelines by Miller [35] for welding thick plates is summarized as follows: (a) weld one pass on one side (side-1) of the built-up box column; (b) flip the built-up box column and weld the other side (side-2) and complete weld passes 1 to 4; (c) flip again and weld side-1 and complete weld passes 2 to 7; (d) flip and weld the other side-2 and complete weld passes 5 to 7; (e) flip and weld the other side-1 and complete weld passes pass 8 to 13; (f) flip and weld the other side-2 and complete weld passes 8 to 13.

The region to be welded and its surrounding area, at a distance equal to 75mm from both sides of the weld, measured from the edge of the weld, was pre-heated to 110 °C as specified by AWS D1.1 “Table 3.2” [2]. A weld pass was then completed with welding temperature of approximately 1500 °C. This weld was left at room temperature for about 20 minutes until the electrodes were returned

to the start position and the weld surface was cleaned. The region surrounding the weld was heated again for the second pass. This pre-heating procedure was followed for all subsequent welds.

After the heavy built-up box columns had cooled to room temperature, they developed cracks near the weld in the direction parallel to the weld axis as illustrated in Figure 2c. These cracks occurred as a result of the high constraint provided by the thickness of the plates, the large amount of heat input required for welding such thickness and the non-homogenous nature of the grain structure of the steel. Additionally, as the plate thickness increases the likelihood of imperfections and defects resulting from the initial rolling process increases [33]. Subsequently, these defects can easily propagate under the high residual stresses generated by the heating and cooling of the steel during welding.

3.4.1 Welding procedure assessment for case study-3

As an application of the FE simulation approach of the welding procedure an assessment was conducted for the case-study heavy built up box column through 3-D FE simulation. Based on feedback from the fabricator the 75mm plates used in the box-column underwent inspection according to AWS D1.1 [2]. Consequently, plates with discontinuities within 3mm from the plate surface and plates with discontinuities at the cut surface greater than 25mm and at more were rejected based on AWS D1.1 [2] clause “5.15.1” for base metal preparation before welding. Applying principles of linear fracture mechanics, with an average upper shelf CVN value of 82 J for specimens taken near the welded area and through the thickness (Table 3), the corresponding fracture toughness of the steel at this area would be $105 \text{ MPa}\cdot\sqrt{\text{m}}$ according to the formula

developed by Barsom and Rolfe [32] shown in Equation 3. An application of the proposed welding simulation is to obtain residual transverse tensile stress values at the region near the weld and through the thickness; which are approximately 350 MPa. This stress level produces a stress intensity factor of 110 MPa. \sqrt{m} for an acceptable surface discontinuity of 25mm and for fracture mode I as shown in Equation 4 [36]. The stress intensity factor is greater than 15% of the fracture toughness of the material at this location; as such, this discontinuity has a 50% chance of propagating as a result of the residual stresses produced from the welding procedure.

$$K_I = \sqrt{0.64 \times CVN \times E} = \sqrt{0.64 \times 82 \times 2.1 \times 10^8} = 105000 \text{ KPa} \cdot \sqrt{m} = 105 \text{ MPa} \cdot \sqrt{m}, \quad (3)$$

$$K = 1.12\sigma\sqrt{\pi a} = 1.12 \times 350 \times \sqrt{\pi \times 0.025} = 110 \text{ MPa} \cdot \sqrt{m}, \quad (4)$$

Where K_I is the dynamic fracture toughness (KPa. \sqrt{m}), CVN is the absorbed energy measured from Charpy-V-Notch tests (Joules) from Table 3, E is the modulus of elasticity of the steel material (KPa) from Table 2, K is the stress intensity factor (MPa. \sqrt{m}), σ is the applied stress level for fracture modes I, II and III (MPa) and a is the crack length (m). Theoretically, by solving the stress intensity formula backward [36] and using the fracture toughness of the material as a stress intensity factor, the resulting discontinuity size becomes 20 mm. As such, for the built-up box column discussed herein any embedded crack of size greater than 20 mm had more than a 50% chance of propagating after the welding procedure has been concluded at the location near the welding area. It is worth mentioning that, according to AWS D1.1 [2], for qualifying a welding procedure for unlimited thickness the test plates need only be 38mm thick. In addition, according to this study and a study conducted by Suwan [37] on the CVN values for different thicknesses of

ASTM A572 Gr.50 [11] steel, the average upper shelf CVN value for plates in the thickness range 19-38mm is about double the value of plates with thickness range of 64-100mm. Accordingly, due to low fracture toughness expected for thick plates (greater than 50mm) as well as higher residual stresses due to welding [6], separate welding specifications and acceptance criteria for welding thick steel plates.

3.5 *Summary of FE model results and validation*

In summary, the FE model of the welding test, developed using the proposed modeling approach (Section 2), was able to predict the measured temperature values from case study 1 as well as the welding residual stress distribution in the 28mm thick box-section measured by Chen and Chang [18] using sectioning method. Furthermore, the FE simulation of the welding procedure for the heavy built-up box column confirmed the propagation of cracks due to the employed welding procedure based on principles of linear elastic fracture mechanics. Hence, the proposed numerical modeling approach can be used for the assessment of welding procedures before they are conducted in order to develop acceptance criteria for the steel plates to be welded. Furthermore, this numerical modeling approach can be used to develop quantitative criteria for establishing better welding procedures and improving existing welding guidelines. The authors are currently working in this direction.

4 Limitations of the proposed modeling approach for welding procedures

It is anticipated that the proposed numerical model would better replicate an automatic welding procedure compared with a manual procedure; this is attributed to the uncertainty in the values of

welding parameters in the case of manual welding, such as the welding speed and the ability of a welder to complete the weld pass as straight as possible. Also, modeling the preheating process parameters, such as the temperature and the preheating period, has to be established as close as possible to their physical values to achieve the most accurate welding simulation. Consequently, welding procedures for which the preheating process is not strictly controlled cannot be simulated accurately at this stage based on the proposed numerical approach. The proposed model is not able to explicitly simulate potential crack propagation; only the residual stress output is provided. Fracture simulation can be introduced in the proposed simulation using the fracture modeling approach developed by Hillerborg et al. [38]. In this case, further validation will be required. Furthermore, the effects of the elevated temperature on the microstructure of steel is not explicitly modeled; to improve the proposed modeling approach the effect of the steel microstructure on the fracture behavior, as illustrated by Manigandan et al. [39], should be considered. The proposed modeling approach is intended for arc welding procedures and cannot be used to simulate other welding procedures such as Oxy-fuel welding; which for example, is conducted by applying very high temperature up to 3500°C to develop a large pool of molten metal.

5 Summary and Conclusions

With the aim of improving guidelines for the welding of thick plates through a practice-oriented evaluation approach a numerical model of the welding procedure was proposed. This modeling approach incorporates a heat transfer analysis followed a stress analysis using the death and birth technique. A mesh sensitivity study was completed and the recommended element sizes are a minimum of 2mm and a maximum of 9mm apply for the 3-D model. The creep strain properties

were introduced in the welding simulation. Two approaches were employed to define the time and temperature dependent strain. For a specific box-column case study, the difference in the stress distribution between the model that accounted for the creep strain properties and the one that did not account for creep was negligible. Tensile coupon and CVN material tests were completed using specimens obtained from different locations in the case-study box columns with the aim of calibrating the numerical model and studying the effect of the welding procedure on the welded plates. These tests demonstrated the extent of the effect of the plate thickness and the welding procedure on the properties of the steel material. The regions near the welded area and the regions through the plate thickness showed lower ductility and fracture toughness than the expected nominal values. In order to validate the results of the numerical model a welding test was carried out of two 75mm thick plates made of the same material as the case study box column. Temperature measurements were obtained during each weld pass at locations close to the welded area, and compared with the results of the numerical model at the same locations. The numerical model was able to predict the measured temperature values with maximum difference of 20% in the temperature values. The resulting residual stress distribution from the proposed method for welding simulation was also validated with experimental results conducted by Chen and Chang [18]. Moreover, based on the CVN test results and by applying the proposed numerical modeling approach on the box column discussed herein it was determined that any discontinuity greater than 0.8mm has more than a 50% chance to propagate under the residual stresses produced from the welding procedure. It can be concluded that the welding of thick plates requires a separate set of welding specifications to reduce residual stresses generated by welding and limit crack sizes and

set minimum upper shelf CVN values near the welding area. The welding simulation can be used to test various automatic submerged arc welding procedures and techniques to determine quantitative guidelines for welding heavy assemblies that utilize thick steel plates.

Acknowledgments

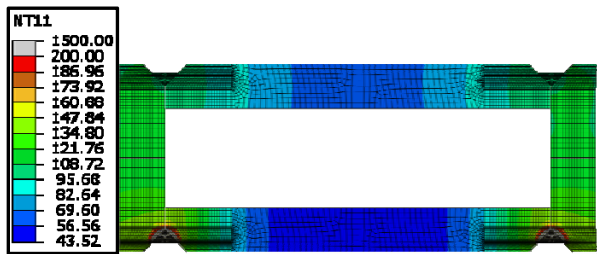
The authors sincerely thank the ADF Group Inc. and DPHV Structural Consultants for their financial and technical support, for providing the tensile and CVN specimens and for carrying out the weld testing. The authors also acknowledge the financial support from the Natural Sciences and Engineering Research Council of Canada.

References

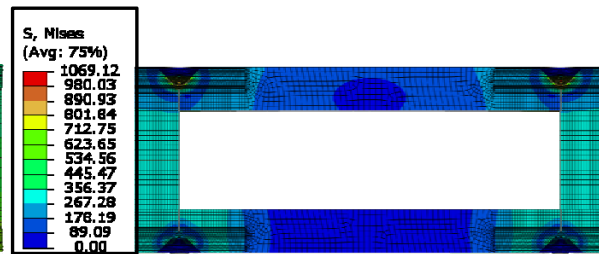
- [1] American Society of Civil Engineers. Minimum design loads for buildings and other structures. Reston, Virginia: Published by American Society of Civil Engineers; 2013.
- [2] AWS D1.1. AWS D1.1 2010. Structural welding code—steel. Miami, FL, USA.: American Welding Society; 2010.
- [3] ANSI/AISC 360-10. AISC 360-10. Specification for structural steel buildings. Chicago, IL, USA.: American Institute of Steel Construction; 2010.
- [4] CAN/CSA-S16-14. Design of steel structures. Mississauga, ON: Canadian Standards Association; 2014.
- [5] CAN/CSA-W59. CAN/CSA W59-13 Welded steel construction. Mississauga, Ont.: Canadian Standards Association; 2013.
- [6] Miller DK. Welding heavy Structural Steel -- Successfully. 2010 NASCC: The Steel Conference. Orlando, FL, USA2010.
- [7] Kamnetzky D. Design and construction failures : lessons from forensic investigations. New York: McGraw-Hill; 1991.
- [8] Bjorhovde R, Brozzetti J, Alpsten GA, Tall L. Residual Stresses in Thick Welded Plates. Weld J. 1972;51:S392.
- [9] ASTM A36. A36 / A36M-14 Standard Specification for Carbon Structural Steel. West Conshohocken, PA: ASTM International; 2014.
- [10] Fisher JW, Pense AW. Procedures for Thermal Cutting and Welding Heavy Structural Shapes. Proceedings of the National Engineering Conference and Conference of Operating Personnel. New Orleans: AISC; 1987. p. 18-1--47.

- [11] ASTM A572 Gr.50. A572/A572M-13a Standard Specification for High-Strength Low-Alloy Columbium-Vanadium Structural Steel. 2013.
- [12] Brickstad B, Josefson BL. A Parametric Study of Residual Stresses in Multi-Pass Butt-Welded Stainless Steel Pipes. *Journal of Pressure Vessel and Piping*. 1998;75:11-25.
- [13] Acevedo C, Drezet JM, Nussbaumer A. Numerical modelling and experimental investigation on welding residual stresses in large-scale tubular K-joints. *Fatigue Fract Eng M*. 2013;36:177-85.
- [14] Nikolaidou V, Rogers CA, Lignos DG. Influence of Welding of Doubler Plates to ASTM A913 450MPa Grade Columns. Eurosteel. Naples, Italy2014.
- [15] ASTM A913 Gr.65. A913/A913M-14a Standard Specification for High-Strength Low-Alloy Steel Shapes of Structural Quality, Produced by Quenching and Self-Tempering Process. 2014.
- [16] Lee C-H, Chang K-H, Do VNV. Finite element modeling of residual stress relaxation in steel butt welds under cyclic loading. *Eng Struct*. 2015;103:63-71.
- [17] Lee J-Y, Kim Y-C, Inose K. Verification of Validity and Generality of Dominant Factors in High Accuracy Prediction of Welding Distortion. *Weld World*. 2010;54:R279-R85.
- [18] Chen S-J, Chang SC. Residual Stresses in Welded Jumbo Box Columns. *Journal of Constructional Steel Research*. 1993;25(3): 201-209.
- [19] Dassault Systemes Simulia Corp. ABAQUS/CAE user's manual. 6.11 ed. RI, USA2011.
- [20] Society of Fire Protection Engineers. SFPE handbook of fire protection engineering. 4th ed. Quincy, Mass. Bethesda, Md.: National Fire Protection Association; 2008.
- [21] British Standards Institution. Eurocode 3: Design of steel structures : Part 1.2 General rules. Structural fire design (together with United Kingdom National Application Document). DD ENV 1993-1-1 : 2001. London: BSI; 2001.
- [22] Hu G, Morovat M, Lee J, Schell E, Engelhardt M. Elevated Temperature Properties of ASTM A992 Steel. *Structures Congress2009*. p. 1-10.
- [23] ASTM A992 Gr.50. A992 / A992M-11, Standard Specification for Structural Steel Shapes. West Conshohocken, PA: ASTM International; 2011.
- [24] Andrade EN. *On the Viscous Flow in Metals, and Allied Phenomena*1910.
- [25] Norton FH. *The Creep of Steel at High Temperatures*: McGraw-Hill Book Company, Incorporated; 1929.
- [26] Faruque MO, Zaman M, Hossain MI. Creep constitutive modelling of an aluminium alloy under multiaxial and cyclic loading. *International Journal of Plasticity*. 1996;12:761-80.
- [27] Johnson AA, Storey RJ. The effect of carbon on the Charpy V-Notch ductile brittle transition curves. ICASI & CCATM'2008 International Conference and Exhibition on Analysis & Testing of Materials. Beijing, China2008.
- [28] Borelli AP, Sidebottom OM. Creep of Metals Under Multiaxial States of Stress. *Nuclear Engineering and Design* 1972;18:415-56.
- [29] Goyal S, Laha K, Das CR, Selvi SP, Mathew MD. Finite element analysis of uniaxial and multiaxial state of stress on creep rupture behaviour of 2.25Cr–1Mo steel. *Materials Science & Engineering A*. 2013;563:68-77.
- [30] Lee J, Morovat MA, Engelhardt MD, Taleff EM. Creep Behavior of ASTM A992 Steel at Elevated Temperatures. In: Fontana M, Frangi A, Knobloch M, editors. 7th International Conference on Structures in Fire. Zurich, Switzerland: ETH Zurich; 2012. p. 95-104.

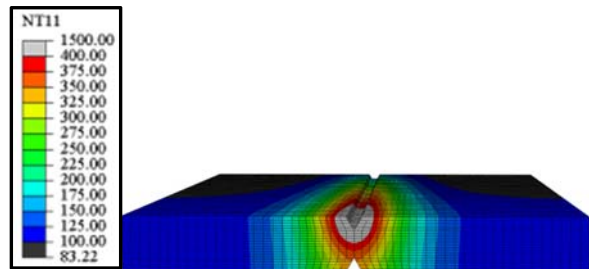
- [31] ASTM A370. A370-14 Standard Test Methods and Definitions for Mechanical Testing of Steel Products. 2014.
- [32] Barsom JM, Rolfe ST. Fracture and fatigue control in structures : applications of fracture mechanics. 2nd ed. Englewood Cliffs, N.J.: Prentice-Hall; 1987.
- [33] Jefferson TB, Woods G. Metals and how to weld them. 2d ed. Cleveland,: James F. Lincoln Arc Welding Foundation; 1962.
- [34] Sundaram P, Pandey RK, Kumar AN. Effect of the Welding Process and Heat Input on the Fracture-Toughness of Welded-Joints in High-Strength Low-Alloy Steel. Mater Sci Eng. 1987;91:29-38.
- [35] Miller DK. AISC Steel Design Guide 21 Welded Connections – A Primer for Engineers. Chicago, IL: American Institute of Steel Construction; 2006.
- [36] Tada H, Paris PC, Irwin GR. The stress analysis of cracks handbook. 3rd ed. New York: ASME Press; 2000.
- [37] Suwan S. Analysis of structural plate mechanical properties : statistical variability and implications in structural reliability [M S in Engineering]: University of Texas at Austin; 2002.
- [38] Hillerborg A, Modeer M, Petersson PE. Analysis of Crack Formation and Crack Growth in Concrete by Means of Fracture Mechanics and Finite Elements. Cement Concrete Res. 1976;6.
- [39] Manigandan K, Srivatsan TS, Quick T, Sastry S, Schmidt ML. Influence of microstructure and load ratio on cyclic fatigue and final fracture behavior of two high strength steels. Materials & Design. 2014;55:727-39.



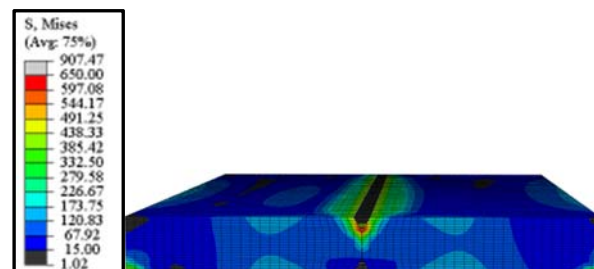
(a) Temperature distribution results from heat transfer simulation of built-up box column after the welding of the sixth pass



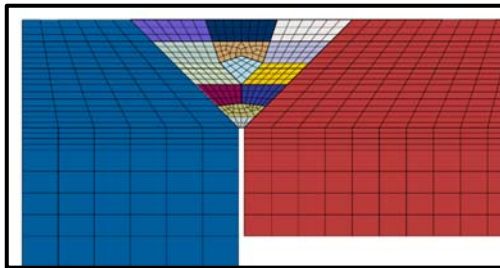
(b) Corresponding Von Mises stress from heat transfer simulation of built-up box column after the welding of the sixth pass



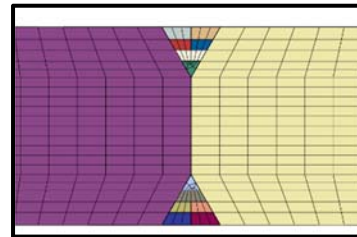
(c) Temperature distribution results from 3D heat transfer simulation of the temperature measuring test after the welding of the second pass



(d) Corresponding Von Mises stress from 3D heat transfer simulation of the temperature measuring test after the welding of the second pass



(e) Finite element mesh at the welding area for the 75mm thick built-up box column model



(f) Finite element mesh at the welding area for the flat welded 75mm thick plates

Figure 1: Finite element simulation of welding procedures in ABAQUS.

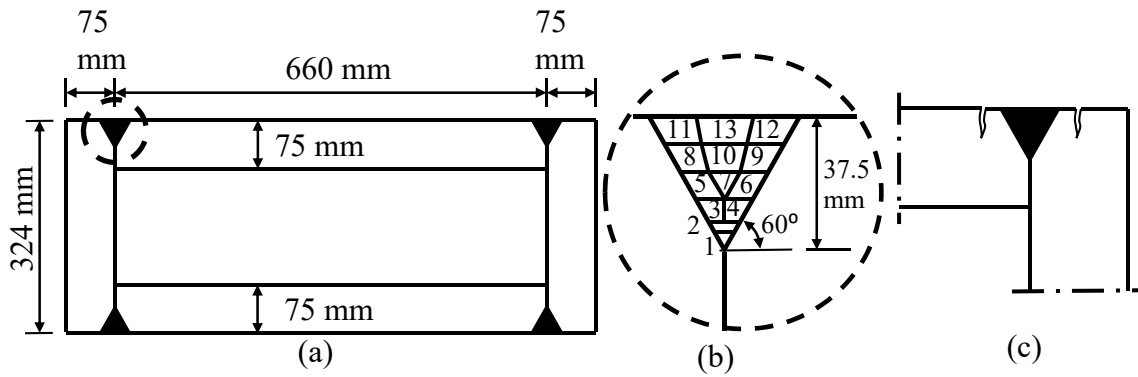


Figure 2: Schematic representation of the PJP welds on the built-up steel box column; a) cross-section dimensions of the built-up box column; b) profile of the welding passes at each partial penetration joint; c) illustration of the location of the cracks that occurred in the case study heavy box column.

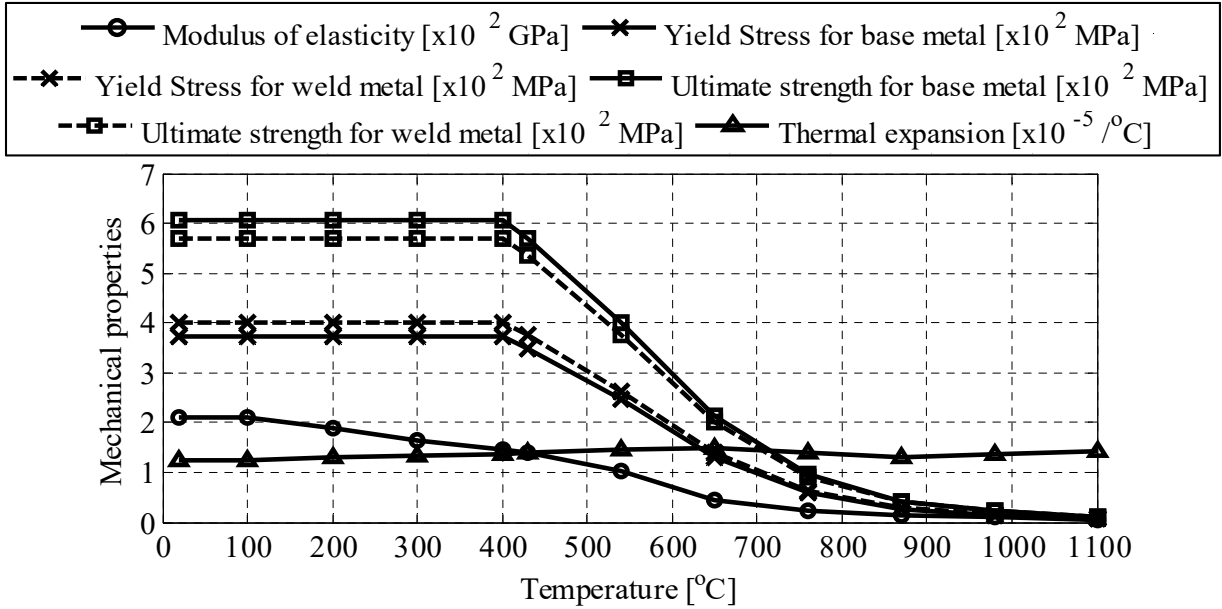


Figure 3: Material properties used in the stress analysis model at elevated temperatures based on AISC 360-10 [3] and SFPE Handbook for fire protection [20].

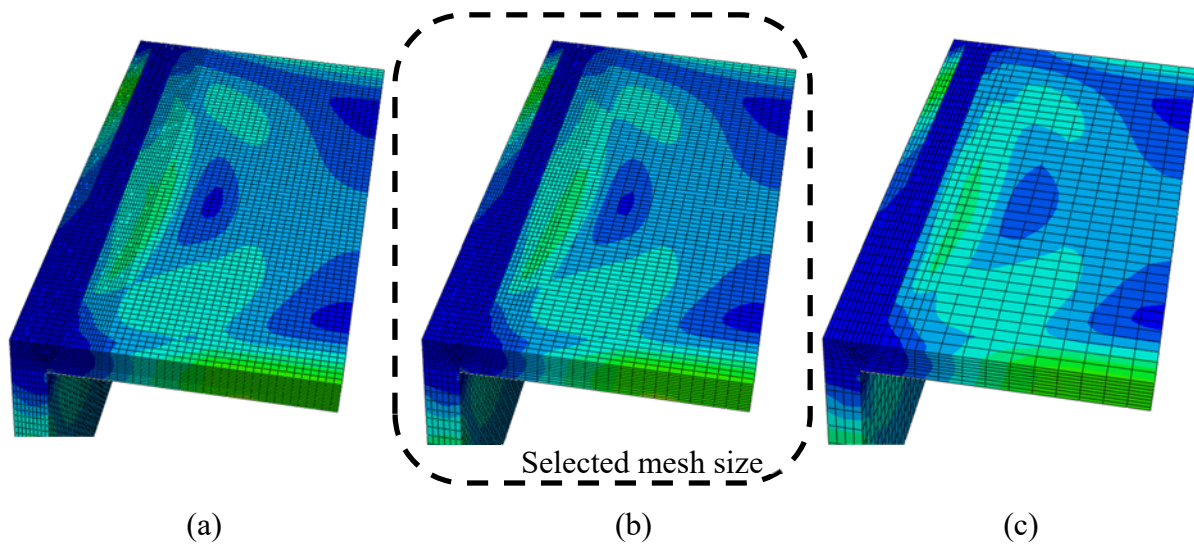


Figure 4: Employed mesh sizes for the FE welding simulation of the 3-D model. a) Maximum element dimension 1 to 5mm, b) Maximum element dimension 2 to 9mm, c) maximum element dimension 5 to 20mm

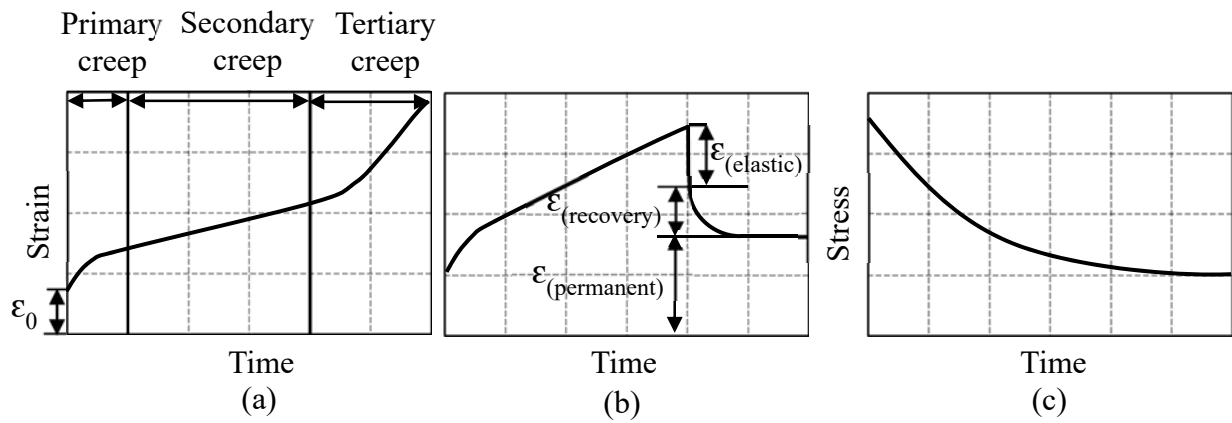


Figure 5: Consideration of creep effects on welding procedures of steel plates; (a) creep strain stages for constant stress and temperature; (b) creep strain recovery; (c) stress relaxation

(adapted from Norton [25]).

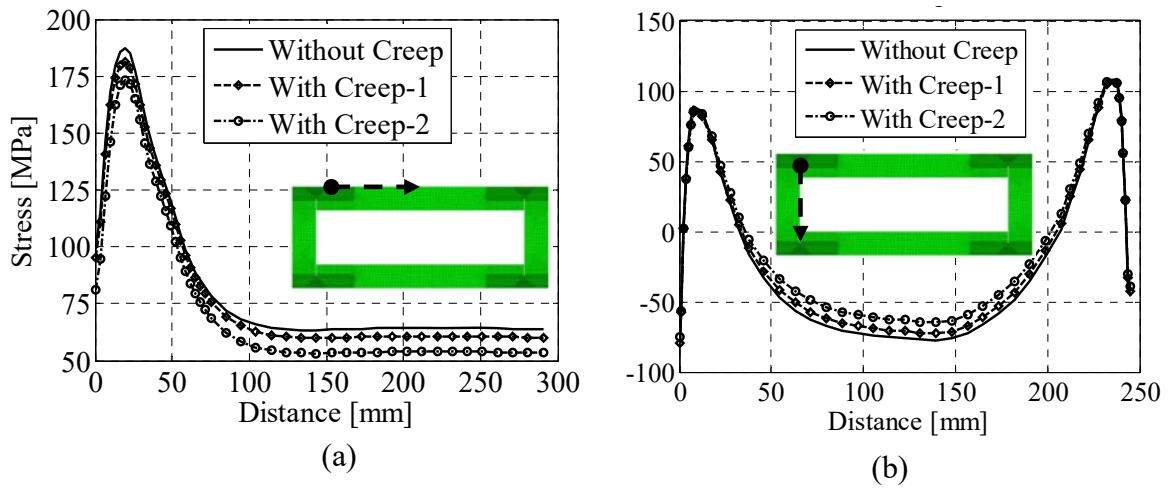


Figure 6: Creep strain effect on the resulting residual stress; (a) transverse stress comparison for creep at horizontal plate after pass number 26; (b) transverse stress comparison for creep at vertical plate after pass number 26.

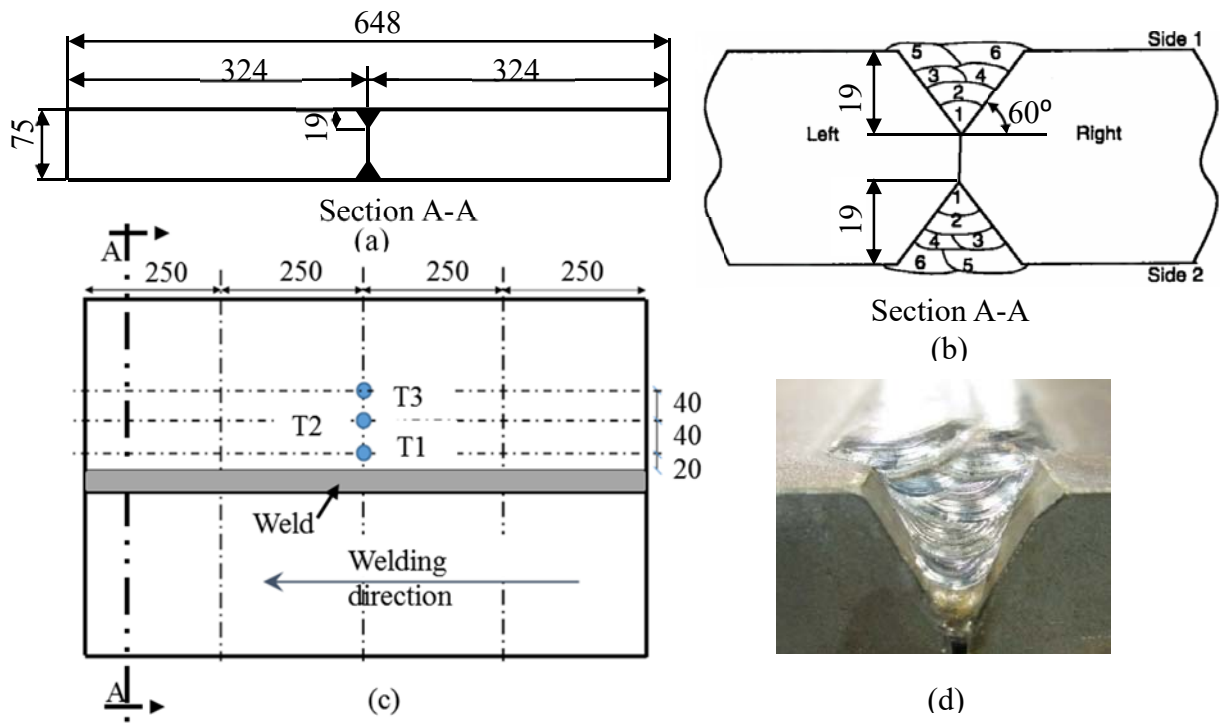


Figure 7: Weld test specimen (dimensions are in mm); (a) cross-section and dimensions of the welded plates; (b) welding sequence conducted for the test; (c) test layout and location of temperature measuring nodes; (d) welded passes after completing the welding process.

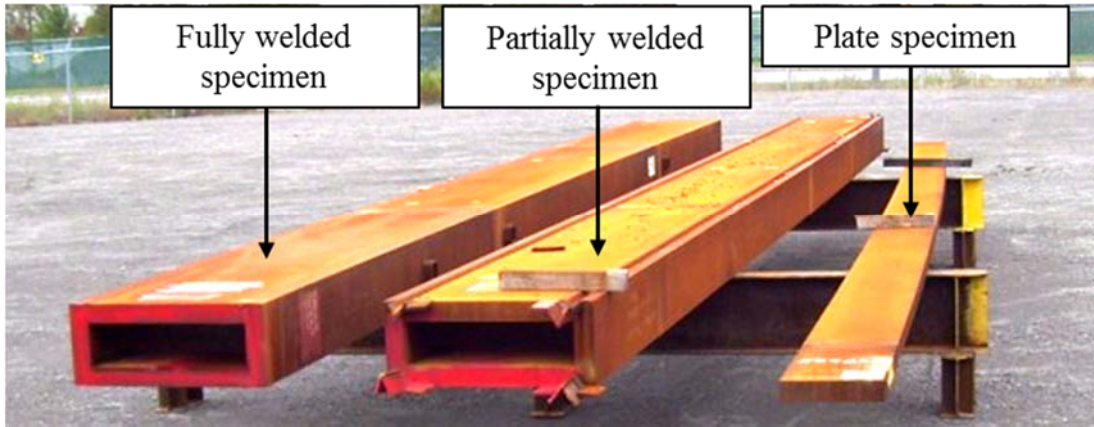


Figure 8: Specimens used for steel material characterization and FE model validation.

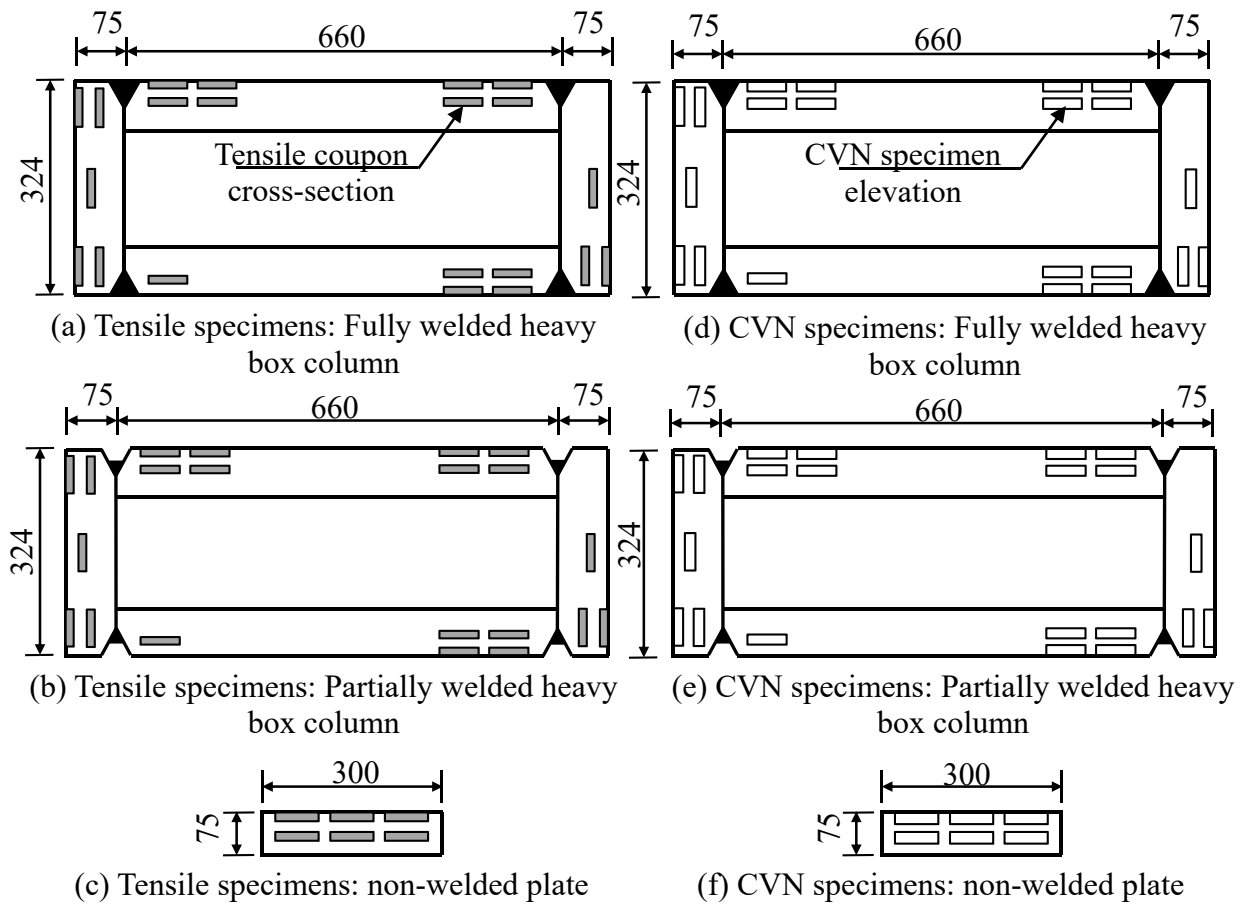
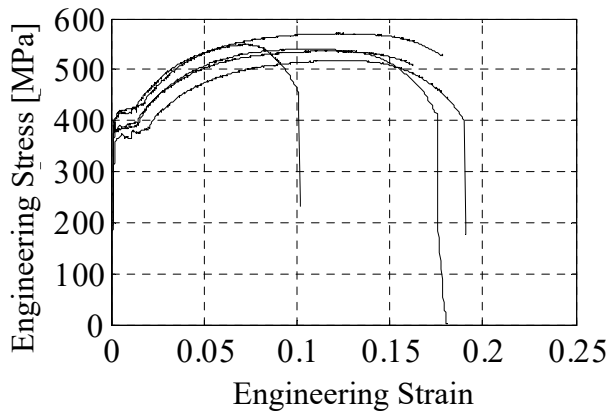
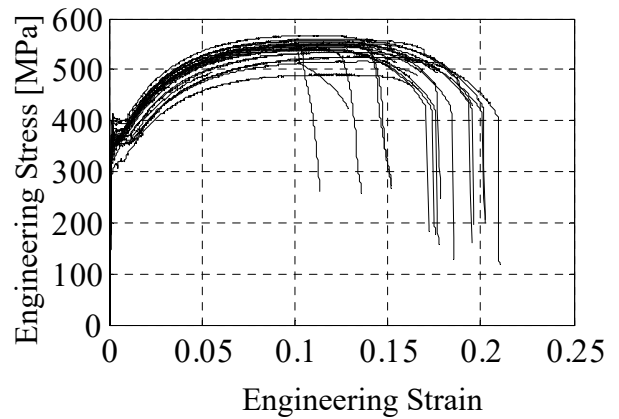


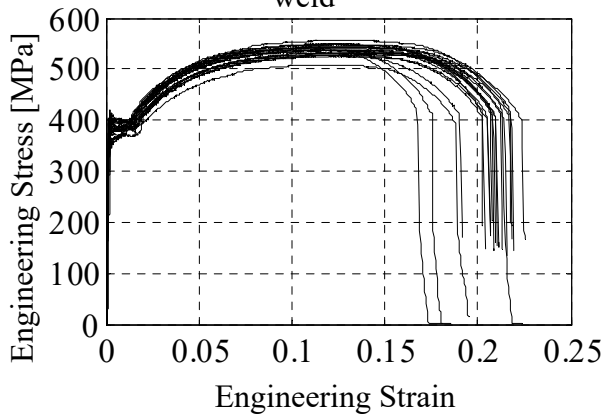
Figure 9: Locations of longitudinal tensile and transverse CVN specimens.



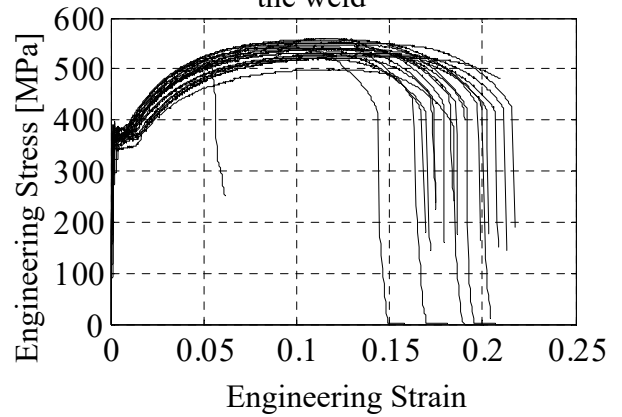
(a) Coupons at plate surface and near the weld



(b) Coupons through the thickness and near the weld



(c) Coupons at plate surface and away from the weld



(d) Coupons through the thickness and away from the weld

Figure 10: Tensile coupon test results for case-study steel plate ($t=75\text{mm}$, ASTM A572 Gr. 50).

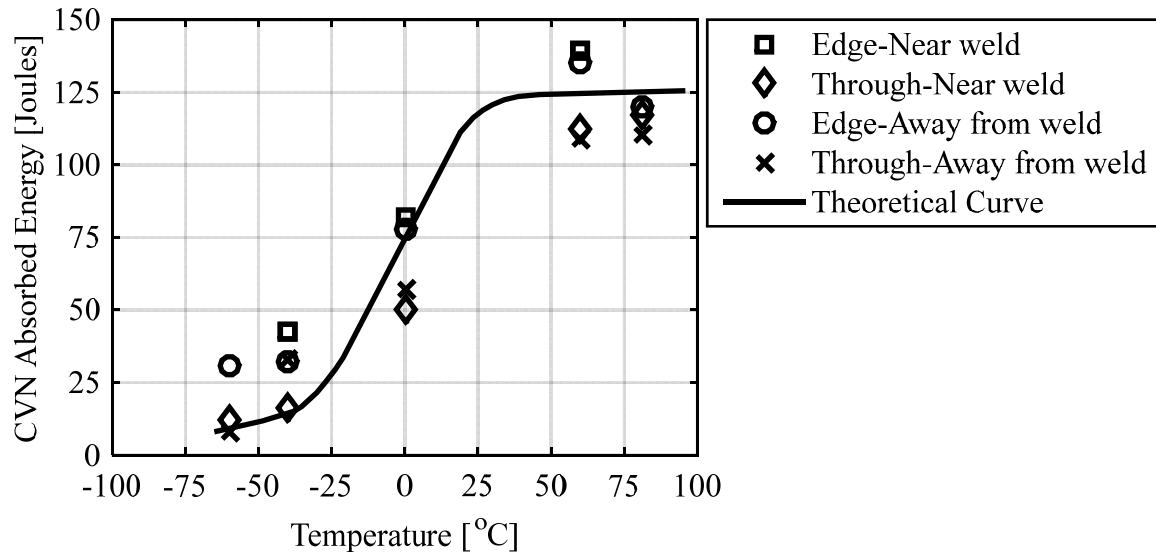
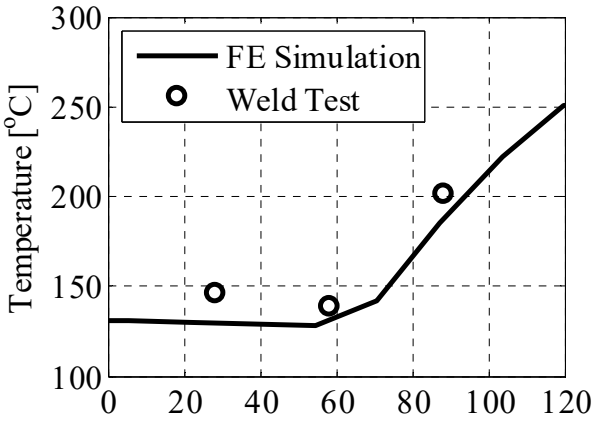
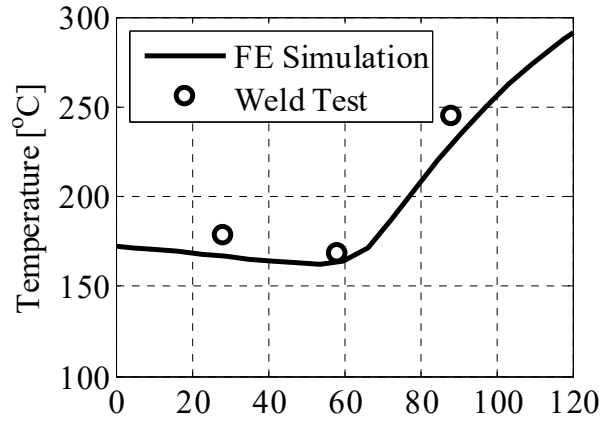


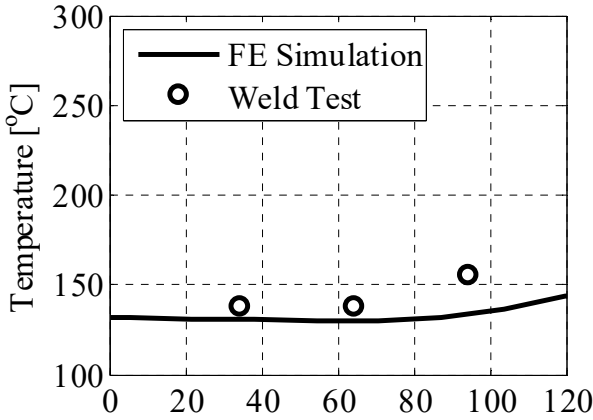
Figure 11: Average CVN absorbed energy values at tested temperatures for different locations in the case-study steel plate ($t=75\text{mm}$, ASTM A572 Gr. 50) and the theoretical CVN-temperature curve according to Johnson and Storey [32].



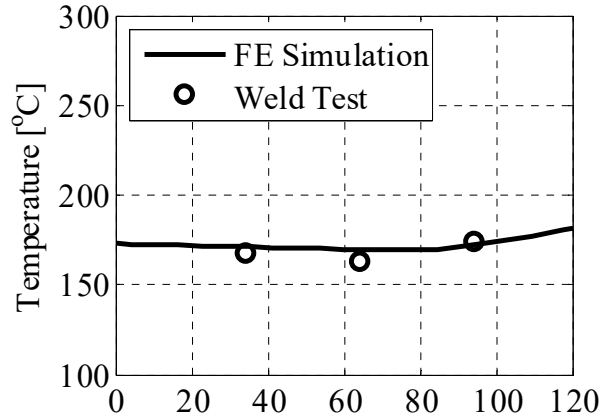
(a) Temperature at node T1 for pass number 3



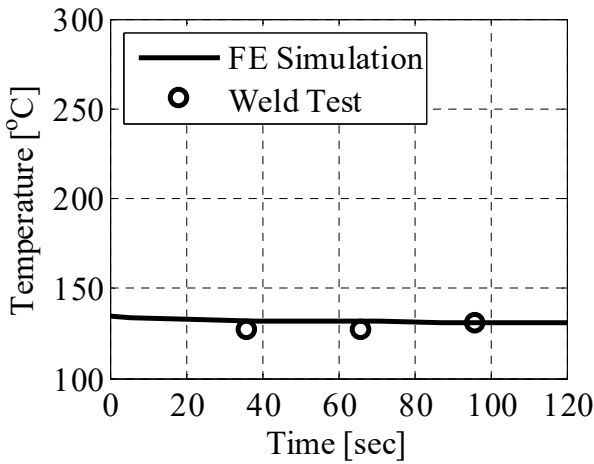
(b) Temperature at node T1 for pass number 5



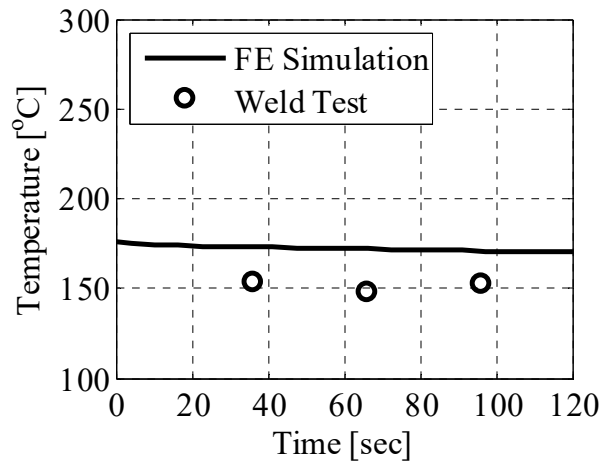
(c) Temperature at node T2 for pass number 3



(d) Temperature at node T2 for pass number 5



(e) Temperature at node T3 for pass number 3



(f) Temperature at node T3 for pass number 5

Figure 12: Comparison of temperature results from the FE simulation and the weld test results.

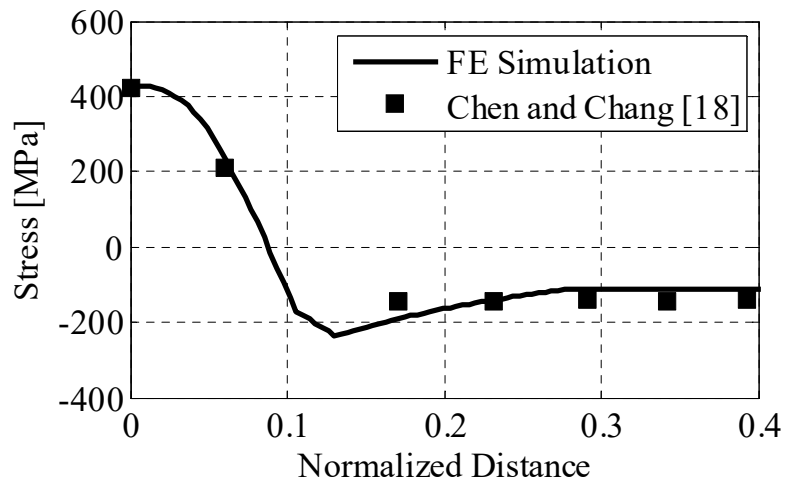
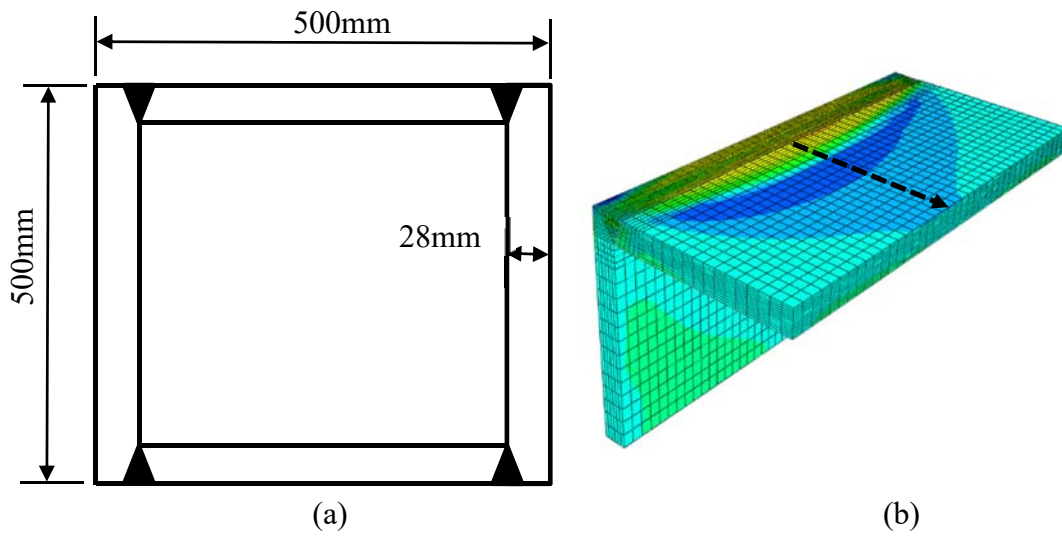


Figure 13: The validation of the residual stress distribution result of the FE simulation with the experimental results from Chen and Chang [18]; a) Dimensions of box section, b) Residual stress distribution from the FE simulation and studied path, c) A comparison between the FE stress distribution results and sectioning method results.

Table 1: Steel material properties at elevated temperatures for heat transfer simulation according to SFPE Handbook of Fire Protection [19]

Required material properties for heat transfer		
T [°C]	Thermal Conductivity [W/m. °C]	Specific heat [N.mm/Kg °C]
20	53.334	4.40E+08
100	50.67	4.88E+08
200	47.34	5.30E+08
300	44.01	5.65E+08
400	40.68	6.06E+08
500	37.35	6.67E+08
600	34.02	7.60E+08
700	30.69	1.01E+09
800	27.36	8.03E+08
900	27.3	6.50E+08
1000	27.3	6.50E+08
1100	27.3	6.50E+08
1200	27.3	6.50E+08

Table 2: Summary of the results of tensile coupon tests for ASTM A572 Gr. 50 steel [11].

	Min	Max	Mean (μ)	St. dev. (σ)	COV
Specimens near the weld and at plate surface					
E [MPa]	198620	234790	211203	16438	8%
f_y [MPa]	355	425	391	39	10%
ϵ_y	0.0017	0.0021	0.0018	0.00017	9%
f_u [MPa]	589	651	609	25	4%
ϵ_u	0.0736	0.1384	0.1199	0.0263	22%
f_u/f_y	1.4246	1.6494	1.5497	0.0860	6%
ϵ_{max}	0.096	0.173	0.1494	0.0309	21%
Specimens near the weld and through the thickness					
E [MPa]	205220	213760	208747	4169	2%
f_y [MPa]	326	338	332	7	2%
ϵ_y	0.0015	0.0016	0.0015	0.00005	3%
f_u [MPa]	522	640	608	26	4%
ϵ_u	0.0543	0.1498	0.1253	0.0206	16%
f_u/f_y	1.3933	1.8253	1.6518	0.1152	7%
ϵ_{max}	0.0543	0.19	0.1520	0.0294	19%
Specimens away from the weld and at plate surface					
E [MPa]	195490	224690	209299	8744	4%
f_y [MPa]	375	411	396	13	3%
ϵ_y	0.0017	0.0020	0.0019	0.0001	6%
f_u [MPa]	576	640	614	16	3%
ϵ_u	0.1110	0.1570	0.1443	0.0110	8%
f_u/f_y	1.4291	1.7815	1.5731	0.1029	7%
ϵ_{max}	0.1610	0.2020	0.1855	0.0104	6%
Specimens away from the weld and through the thickness					
E [MPa]	192950	222870	202281	8248	4%
f_y [MPa]	344	387	365	14	4%
ϵ_y	0.0015	0.0019	0.0018	0.0001	7%
f_u [MPa]	518	634	595	34	6%
ϵ_u	0.0516	0.1660	0.1273	0.0226	18%
f_u/f_y	1.4066	1.7802	1.5986	0.1027	6%
ϵ_{max}	0.0592	0.1990	0.1645	0.0302	18%

Table 3: Summary of the CVN results for ASTM A572 Gr. 50 steel [11].

Temperature [°C]	Min [J]	Max [J]	Mean (μ) [J]	St. dev. (σ) [J]	COV
Specimens near the weld and at plate surface					
-40	41	44	42.5	2.1	5%
0	74	90	82	11.3	14%
60	135	143	139	5.7	4%
Specimens near the weld and through the thickness					
-60	4	20	12	8.1	67%
-40	14	20	16	3.2	21%
0	35	64	50	12.1	24%
60	98	128	112	8.7	9%
81	93	131	117	15.9	16%
Specimens away from the weld and at plate surface					
-60	13	45	31	16.5	53%
-40	22	79	32	21.6	68%
0	67	102	78	13	17%
60	117	157	135	10.6	8%
81	104	141	120	12.8	11%
Specimens away from the weld and through the thickness					
-60	4	12	8	4.1	51%
-40	14	101	33	34.8	105%
0	34	78	57	19.4	34%
60	87	159	109	21.3	20%
81	86	136	110	15.8	14%